Icarus xxx (2009) xxx–xxx

Contents lists available at ScienceDirect

Icarus

journal homepage: www.elsevier.com/locate/icarus

Convective cloud heights as a diagnostic for methane environment on Titan

Erika L. Barth *, Scot C.R. Rafkin

Southwest Research Institute, 1050 Walnut Street, Suite 300, Boulder, CO 80302, United States

ARTICLE INFO

Article history:
Received 12 June 2008
Revised 5 December 2008
Accepted 19 January 2009
Available online xxxx

Keywords:
Titan
Atmospheres
Structure

ABSTRACT

The appearance of convective clouds in Titan's troposphere has been documented from ground-based observation for more than a decade. Cloud tops have been reported between 14 and 25 km. Higher resolution Cassini data have shown smaller portions of the cloud system can reach up to 42 km. We use the Titan Regional Atmospheric Modeling System (TRAMS) to explore environments which allow convective clouds to reach the tropopause. In general, cloud tops remain below 30 km, but for environments where the surface humidity of methane is greater than 50%, a small portion at the center of the cloud rises briefly to higher altitudes; for $\geqslant$65% humidity, the cloud top reaches nearly to the tropopause ($\sim$40 km). A number of other parameters also have noticeable affects on cloud top such as nucleation critical saturation, haze abundance, and collisional growth of cloud particles.

1. Introduction

Clouds in Titan's atmosphere are now well observed phenomena. Griffith et al. (1998) initially discovered clouds in Titan's atmosphere from disk integrated spectra. Their observations pointed to a large cloud system covering about 14% of Titan's disk, with cloud tops around 14 km and a lifetime of more than a day. Although they could not spatially resolve the cloud, they believed it to be near equatorial latitudes. Their next set of observations was able to see smaller and rapidly changing (hours) clouds, which they located at approximately 25 km altitude, but still could not place in latitude.

Titan's south pole cloud activity was first imaged in 2001 (Roe et al., 2002), which corresponds to approximately 1 terrestrial year before southern summer solstice (a Titan season is slightly less than 7.5 terrestrial years). The south polar cloud system is long-lived, though individual clouds may form and dissipate rapidly. Over long timescales, the clouds vary from small, sporadic bursts to large storm systems (Schaller et al., 2006a). Most observations have placed the tops of these clouds in the troposphere, but did not provide a precise altitude. However, Brown et al. (2002) reported an altitude of 16 ± 5 km for cloud tops observed over a 2-day period in Dec. 2001. Their observations can be fit by a single 200 km diameter cloud or an equivalent group of smaller clouds. In a later set of their observations, a larger cloud, horizontally extending $\approx$1400 km, was observed. Bouchez and Brown (2005) reported on south polar clouds between 100 and 400 km in diameter which persisted over 2–3 nights. Roe et al. (2002) also observed over a three day period and reported seeing temporal variability. They give a minimum area for each cloud system spanning 20,000 to 70,000 km^2 (for 6 cloud systems). The large storm seen by Schaller et al. (2006b) lasted between 25 and 30 days and appears to be a number of storms forming in quick succession.

The first mid-latitude clouds were observed in 2003 (Roe et al., 2005a). These clouds were all located near 40° latitude and were originally thought to be confined to a specific longitude, though recent observations have shown the clouds to be more variable in longitude. Clouds often appear in groups and tend to be extended in longitude, several hundred to several thousand kilometers. Individual cloud lifetimes are of order 1 (terrestrial) day, but could be longer for smaller clouds below the resolution limit of 300 km (Roe et al., 2005b). No altitude data was reported from the ground-based observations.

The first Cassini observations of clouds were reported by Porco et al. (2005). They reported three classes of clouds seen by the Imaging Science Subsystem (ISS); small-scale bright clouds near the south pole, smaller and shorter lived mid-latitude clouds, and larger scale nearly zonal streak clouds at latitudes ranging from 14° S to 72° S. Of these cloud classes, ground-based and additional Cassini observations point to the first two being convective in origin. The zonally extended clouds are not clearly convective and may be stratiform. Barth and Rafkin (2007) showed that stratiform clouds are likely to form given Huygens landing site conditions.

Griffith et al. (2005) reported on four mid-latitude clouds observed by Cassini's Visual and Infrared Mapping Spectrometer (VIMS). Each of the clouds was seen to rise rapidly to the tropopause (from $\sim$20 to 42 km in 35 min) and then dissipate or fall 10 km within half an hour. Some horizontal growth ($\sim$50 km distance within 1 h) was also seen following the updrafts. Three

* Corresponding author. Fax: +1 (303) 546 9687.
E-mail address: ebarth@boulder.swri.edu (E.L. Barth).

0019-1035/$ - see front matter © 2009 Elsevier Inc. All rights reserved.
doi:10.1016/j.icarus.2009.01.032

Table 1
Variables in equations.

Variables in mass continuity equation (Eq. (1))	
Π'	Exner function
c_v	specific heat capacity at constant volume
ρ	air density
$\mathbf{u}$	velocity
S	source term to account for phase changes
θ_v	virtual potential temperature
Variables in microphysics equations (Eqs. (2) and (3))	
n	particle number density
v_{fall}	fall velocity
K_{coag}	coagulation kernel
v	particle volume
P	production term for haze particles
L	loss term for haze particles
J	nucleation rate
G	condensation(evaporation) rate
Variables in droplet heat transfer equations (Eqs. (4)–(9))	
k_{drop},k_{air}	thermal conductivity of droplet, air
T_{drop},T_{air}	temperature of droplet, air
$T_0{}^*$	triple point temperature of condensate
r,r_{ice}	radius of droplet, ice core in droplet
f_t,f_v	ventilation factors
D_v	diffusivity
M	molecular weight of condensate
$\mathscr{R}$	universal gas constant
e_∞,e	vapor pressure (saturation, partial)
L_{evap},L_{melt}	latent heat of evaporation, melting
$\frac{dm}{dt}$	growth rate of particle from condensation (evaporation)
Variables in coagulation equations (Eqs. (10)–(12))	
E_{coal},E_{coll}	coalescence, collision efficiency
r_l,r_s	radius of large, small colliding particle
v_{fl},v_{fs}	fall velocity of large, small colliding particle
$f(y)$	function of ratio (y) of colliding particles
We	Weber number
ρ_{drop}	density of droplet
σ_{lv}	droplet surface tension

of the clouds showed multiple centers of activity. The overall conclusion was that they were seeing evidence of vigorous convection followed by rainout and movement through zonal wind transport.

Remote observations cannot see the microphysical processes at work in the clouds, yet these processes influence the lifetime and appearance of the clouds. A number of microphysical parameters which are still poorly constrained include properties of the cloud condensation nuclei such as abundance and size of haze particles and the critical saturation for methane nucleation, properties of the cloud particles such as the efficiency for coalescence, and properties of the environment such as the amount of methane in the atmosphere. Hueso and Sánchez-Lavega (2006) performed a study, varying haze and methane abundance, triggering mechanism and coalescence efficiency in their 3-D methane convection model. They found a cloud lifetime totalling about 10 hours and cloud top heights were generally below 30 km. We present here a number of simulations from our regional scale convection model, the Titan Regional Scale Atmospheric Modeling System (TRAMS). Our study covers a wider range of parameter space and is able to more closely match observations with higher cloud tops.

TRAMS and initial simulations were described in Barth and Rafkin (2007); we present a further description and subsequent model improvements in Section 2. Section 3 describes simulation results in a number of methane environments in order to best match the observations of Griffith et al. (2005), followed by further tests to understand the sensitivity of various poorly constrained parameters (e.g. haze abundance, critical saturation, coalescence efficiency). A discussion of the best scenarios for reproducing ground-based and Cassini observations as well as the implication for rainfall is given in Section 4. We conclude in Section 5.

2. The microphysics model

TRAMS is a coupled regional-scale dynamic and column microphysics model. The governing equations for the dynamical core are the standard non-hydrostatic Reynolds-averaged primitive equations and are the same as those given in (Rafkin et al., 2001; Eqs. (1)–(6)), except as described below. In TRAMS, the heating term in the thermodynamics equation describes latent heat release during cloud formation/dissipation; radiative forcing is turned off as the timescale of radiative heating in Titan's troposphere is long compared to hourly timescales associated with convection. The quantities in the tracer continuity equation include methane vapor, haze particles, and cloud particles. The mass continuity equation,

$$\frac{\partial \Pi'}{\partial t} = \frac{-\mathscr{R}\Pi}{c_v \rho}\left[\nabla \cdot (\rho \mathbf{u}) - S\right] + \frac{\mathscr{R}\Pi}{c_v \theta_v}\frac{\partial \theta_v}{\partial t} \tag{1}$$

differs from that given in Rafkin et al. (2001) with the inclusion of a thermal compression term (Nicholls and Pielke, 2000). Table 1 describes the terms in Eq. (1).

The microphysics package was adapted from Barth and Toon (2006) and operates independently on each column. The model solves the continuity equation for a particle n of volume v, with the form

$$\frac{\partial n}{\partial t} = -\frac{\partial}{\partial z}(n v_{\text{fall}}) + \frac{1}{2}\int_0^v K_{\text{coag}}(v', v - v')n(v')n(v - v')dv' - \int_0^\infty K_{\text{coag}}(v', v)n(v)n(v')dv' + P(v) - L(v) \tag{2}$$

for aerosol particles, and

$$\frac{\partial n}{\partial t} = -\frac{\partial}{\partial z}(n v_{\text{fall}}) + \frac{1}{2}\int_0^v K_{\text{coag}}(v', v - v')n(v')n(v - v')dv' - \int_0^\infty K_{\text{coag}}(v', v)n(v)n(v')dv' + J(v) - \frac{\partial}{\partial v}(G(v)n(v)) \tag{3}$$

for cloud particles. Both haze and cloud particles are subject to sedimentation (first term in each equation above). Transport of particles by advection (the dominant transport process for the smaller haze particles) and diffusion is handled by the TRAMS dynamics model, outside the microphysics. Term 2 in both equations describes growth through coagulation, Brownian for haze and gravitational collection for clouds. Clouds can also scavage haze particles, but this represents a negligible loss process for the haze. Haze production, $P(v)$, is through a flux supplied at model top or describes evaporation of clouds and haze loss, $L(v)$, is through nucleation. Cloud production, $J(v)$, is through nucleation and $G(v)$ describes condensation/evaporation.

Methane clouds in Titan's atmosphere are likely to be composed of both ice and liquid (methane diluted with nitrogen and possibly other hydrocarbons) particles. The freezing point of a mixture of methane with about 20% nitrogen occurs at 80.6 K, or above about 15 km. Thompson et al. (1992) noted that as the N_2/CH_4 mixture freezes some nitrogen will be exsolved, changing the melting point of the ice particles to be higher than the freezing point of the more dilute liquid mixture. A pure methane ice crystal melts when temperature rises above 90.6 K, which occurs for altitudes below about 5 km. Graves et al. (2008) noted that evaporative cooling of falling ice particles is sufficient to keep the particle's temperature above a melting point of 90.6 K for the time it takes the particle to completely evaporate or fall the 5 km to the surface. In Barth and Rafkin (2007) we used a fixed rate for both melting and freezing of cloud particles when they reached a temperature of 80.6 K. Here

Please cite this article in press as: Barth, E.L., Rafkin, S.C.R. Convective cloud heights as a diagnostic for methane environment on Titan. Icarus (2009), doi:10.1016/j.icarus.2009.01.032

we now track the temperature of the cloud particle, similar to Graves et al. (2008).

The droplet temperature can be found by equating the rate of heat transfer through the liquid layer to the ice core to the rate of heat transfer through air to the particle surface by forced convection and evaporation(condensation),

$$\frac{4\pi k_{\mathrm{drop}}(T_{\mathrm{drop}}-T_0)rr_{\mathrm{ice}}}{r-r_{\mathrm{ice}}} = 4\pi r k_{\mathrm{air}}(T_{\mathrm{air}}-T_{\mathrm{drop}})f_t + \frac{4\pi r D_v f_v M}{\mathscr{R}}\left[\frac{e_\infty}{T_{\mathrm{air}}}-\frac{e}{T_{\mathrm{drop}}}\right]L_{\mathrm{evap}}. \quad (4)$$

Solving for droplet temperature gives,

$$T_{\mathrm{drop}} = \frac{\xi_1 T_0 + \xi_2 T_{\mathrm{air}} + \xi_3}{\xi_1+\xi_2}, \quad (5)$$

where

$$\xi_1 = k_{\mathrm{drop}} r_{\mathrm{ice}}, \quad (6)$$

$$\xi_2 = k_{\mathrm{air}} f_t (r - r_{\mathrm{ice}}), \quad (7)$$

$$\xi_3 = \frac{dm}{dt} L_{\mathrm{evap}} \frac{r-r_{\mathrm{ice}}}{4\pi r}, \quad (8)$$

Then, assuming a steady-state and no internal circulation in the melt, the mass change of the ice core is found from

$$L_{\mathrm{melt}} \frac{dm_i}{dt} = \frac{4\pi r r_{\mathrm{ice}} k_{\mathrm{drop}}(T_0 - T_{\mathrm{air}})}{r - r_{\mathrm{ice}}}, \quad (9)$$

which equates the rate of release of latent heat to the rate of heat transfer through the liquid layer. Table 1 describes the variables in Eqs. (4)–(9) above.

The complete model is run in two dimensions with a vertical extent of 50 km and a horizontal extent of 500 km. Vertical layers are spaced beginning with 15 m near the surface and increase with altitude until reaching a constant 2 km above 16 km. Horizontal spacing is 1 km. The horizontal boundary condition is cyclic. The top boundary of the model allows a flux of haze particles into the model; the bottom boundary allows for loss of particles through precipitation. The atmosphere is initialized horizontally homogeneously using the temperature–pressure profile measured by the HASI instrument on the Huygens probe (Fulchignoni et al., 2005). The u and w velocity components are initialized to zero. A number of methane profiles are constructed as shown in Fig. 1: Given a fixed surface humidity, the methane abundance follows a constant mixing ratio until saturation is reached; then the curve follows saturation (with respect to the binary mixture of liquid $CH_4 + N_2$ as given by Thompson et al., 1992) until a minimum value is reached and the mixing ratio becomes constant again.

3. Model results and sensitivity tests

A warm bubble placed at the surface in the center of the model domain initiates the rising of an air parcel. In general, we use a gaussian shaped bubble with a temperature amplitude of 3 K. The dimensions of the bubble are small compared to the spatial scales of the clouds which later form. The 3 K perturbation only extends ± 1 (kilometer) grid box horizontally and up to about 200 m in z. Outside of $x = \pm 10$ km from the center and $z \lesssim 240$ m, Titan's temperature profile is unaffected. The 3 K bubble temperature was chosen as it is sufficiently buoyant to initiate cloud formation within the first two hours (times refer to terrestrial unless otherwise indicated) of simulation time, but is a small enough thermal perturbation compared to later effects from condensation. For instance, heat effects from the bubble at 1 km (the lowest lifting condensation level in these simulations) are less than 0.1 K at the time a cloud first forms, whereas latent heat release from condensation warms the air by several Kelvin.

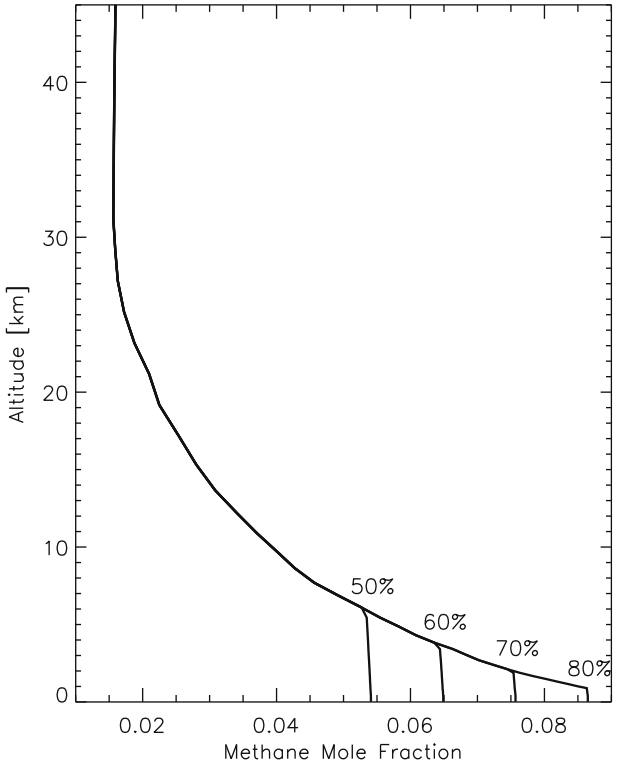

Fig. 1. Constructed methane mole fraction profiles used for initializing TRAMS. Relative humidity is indicated for each curve (RH numbers are given with respect to pure liquid CH_4, however the vapor pressure curve includes the effects of the binary mixture of $CH_4 + N_2$ in order to insure model initialization with subsaturated conditions). For comparison, the mole fraction of methane found at the surface by the Huygens probe is 4.92×10^{-2}.

Table 2
Characteristics of clouds as a function of methane environment.

	50%	60%	70%	80%
Cloud Base (LCL)	4.3 km	3.0 km	1.9 km	0.9 km
Level of Free Convection (LFC)	6.8 km	4.9 km	2.7 km	1.5 km
Equilibrium Level	24 km	28 km	30 km	32 km
Approx. initial CAPE	200 J/kg	540 J/kg	900 J/kg	1300 J/kg
Maximum Cloud Top Altitude[a]	28–30 km	32–34 km	36–38 km	36–38 km
Time at max vertical extent	4 hrs	2 hrs	1 hr	2 hrs
Max Horizontal Extent at 10 km	180 km	350 km	500 km	500 km
Max Horizontal Extent at 20 km	120 km	270 km	320 km	500 km
Max Horizontal Extent at 30 km	-	180 km	200 km	250 km
Maximum Updraft Velocity	9 m/s	18 m/s	20 m/s	20 m/s

[a] At VIMS resolution.

Cooler bubbles are sufficient to trigger convection for the environments considered here (e.g. with more methane than the Huygens landing site) but require longer integration time before convective onset with little change in the result. We have explored bubble temperatures down to 1/4 K. For bubbles $\leqslant$1 K, multiple clouds form simultaneously and their competing effects result in a lower peak cloud top by 1–2 vertical levels ($\sim$2–4 km). A similar effect is seen when the model is initialized by random temperature perturbations in the lowest 250 m and spread across the entire x-domain.

3.1. Environments which allow convection

The only true sounding for Titan's atmosphere was at the Huygens landing site near -10° latitude. No optically thick clouds

Please cite this article in press as: Barth, E.L., Rafkin, S.C.R. Convective cloud heights as a diagnostic for methane environment on Titan. Icarus (2009), doi:10.1016/j.icarus.2009.01.032

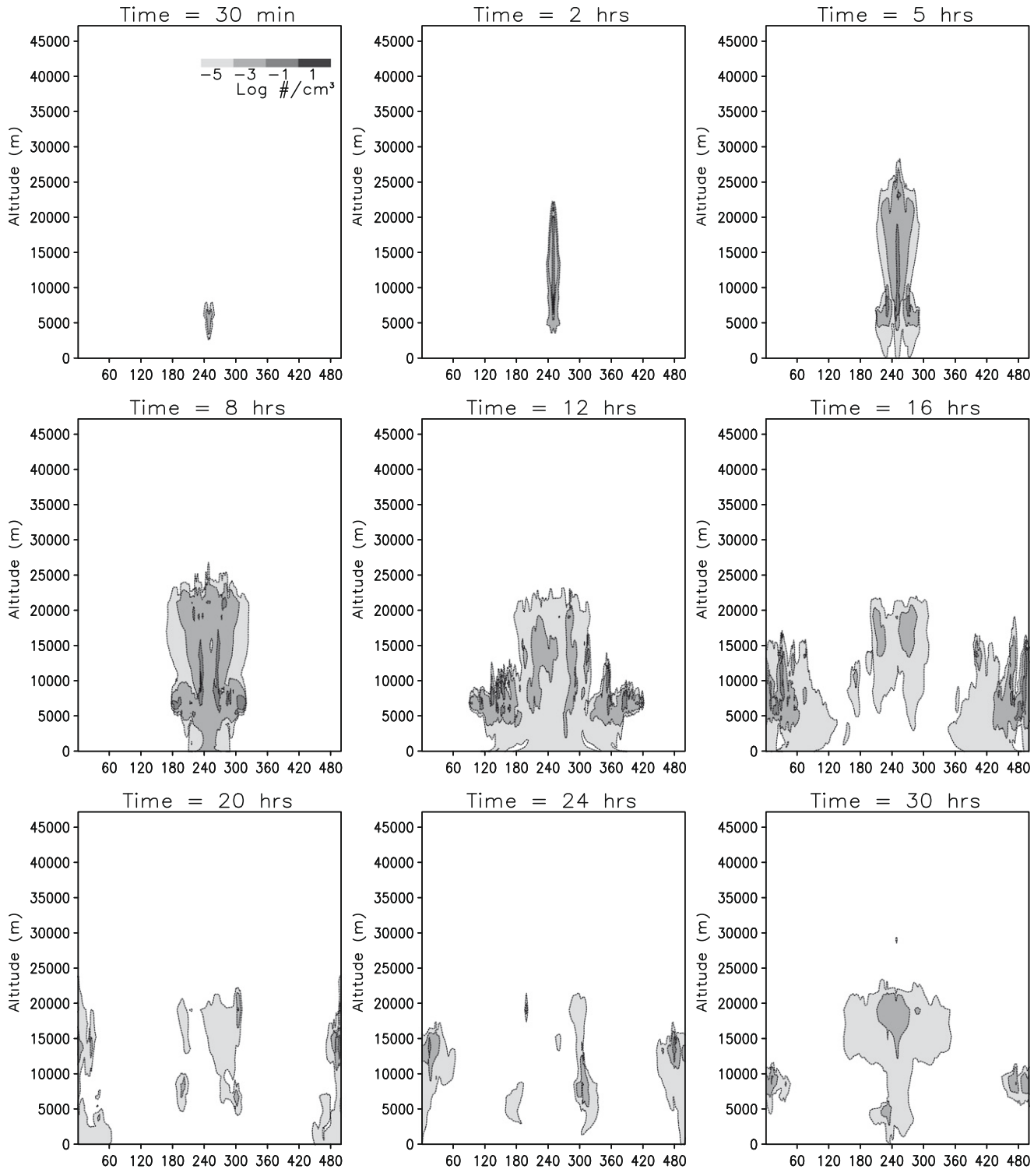

Fig. 2. Time evolution of clouds from a TRAMS simulation. The model was initialized with a 3 K warm bubble at $x = 250$ km in an atmosphere defined by the Huygens temperature- pressure profile and a methane surface humidity of 50%. Contours show the number density of cloud particles (number density in cm^{-3}). Contour labels are log of number density (-5, -3, -1, 0, 1); shading darkens with increased number. The shading is consistent for all plots. Clouds are below optical depth of 0.1 for $N \lesssim 10^{-3}$ cm^{-3}.

have been observed here. Barth and Rafkin (2007) could only form stratiform clouds here and noted that the environment would require a higher methane abundance than was measured in order to form convective clouds, particularly if they were to be observable to Cassini and ground-based telescopes. Here we show that the maximum vertical extent of the clouds is most strongly tied to the methane abundance. Table 2 summarizes properties of the clouds as a function of methane relative humidity at the surface.

Once nucleation begins, the clouds tend to go through a general life cycle, independent of the methane abundance. This process is illustrated for the four different methane cases in Figs. 2–5. First a narrow (few km extent) cloud forms in the center of the model domain and rapidly rises. It takes about 30 min for the top of the

Please cite this article in press as: Barth, E.L., Rafkin, S.C.R. Convective cloud heights as a diagnostic for methane environment on Titan. Icarus (2009), doi:10.1016/j.icarus.2009.01.032

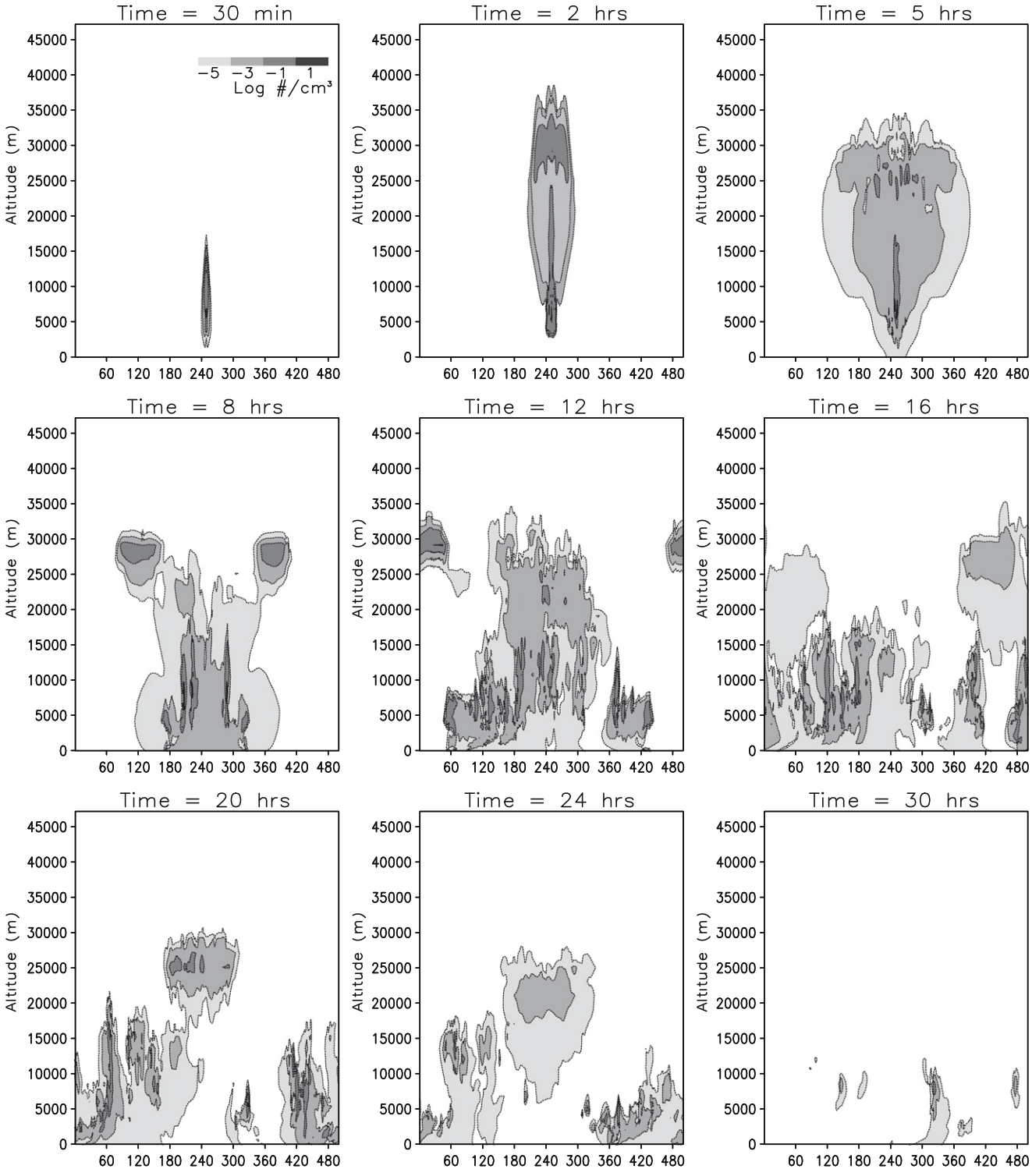

Fig. 3. Time evolution of clouds from a TRAMS simulation for a model initialized with a methane surface humidity of 60%. Contours are the same as in Fig. 2.

cloud to reach 15 km where temperatures are cold enough for methane ice to form. The cloud top continues to rise until briefly reaching its peak altitude, then falling to a lower cloud top. This all happens within about 3 h after initial cloud formation. Sporadic narrow plumes (only a few kilometers in extent, so below even Cassini resolution) continue to rise to high altitudes, but the observable portion of the cloud spreads horizontally with a cloud top at a lower altitude forming an anvil. Precipitation reaches the surface, mainly below the center of the cloud. Additional clouds form at lower altitudes, moving horizontally outward from the central cloud. This phenomenon is seen in terrestrial thunderstorms where new cells are generated along the gust front, which can also cut off older cells from their supply of buoyant air. The central cloud disappears entirely within the first 24 h, but additional cloud formation occurs throughout the 500 km model domain in x, generally below 15 km in z, but sometimes at higher altitudes. Some stratiform cloud formation is seen, centered horizontally, after the initial central storm has dissipated. These clouds are triggered as the air

Please cite this article in press as: Barth, E.L., Rafkin, S.C.R. Convective cloud heights as a diagnostic for methane environment on Titan. Icarus (2009), doi:10.1016/j.icarus.2009.01.032

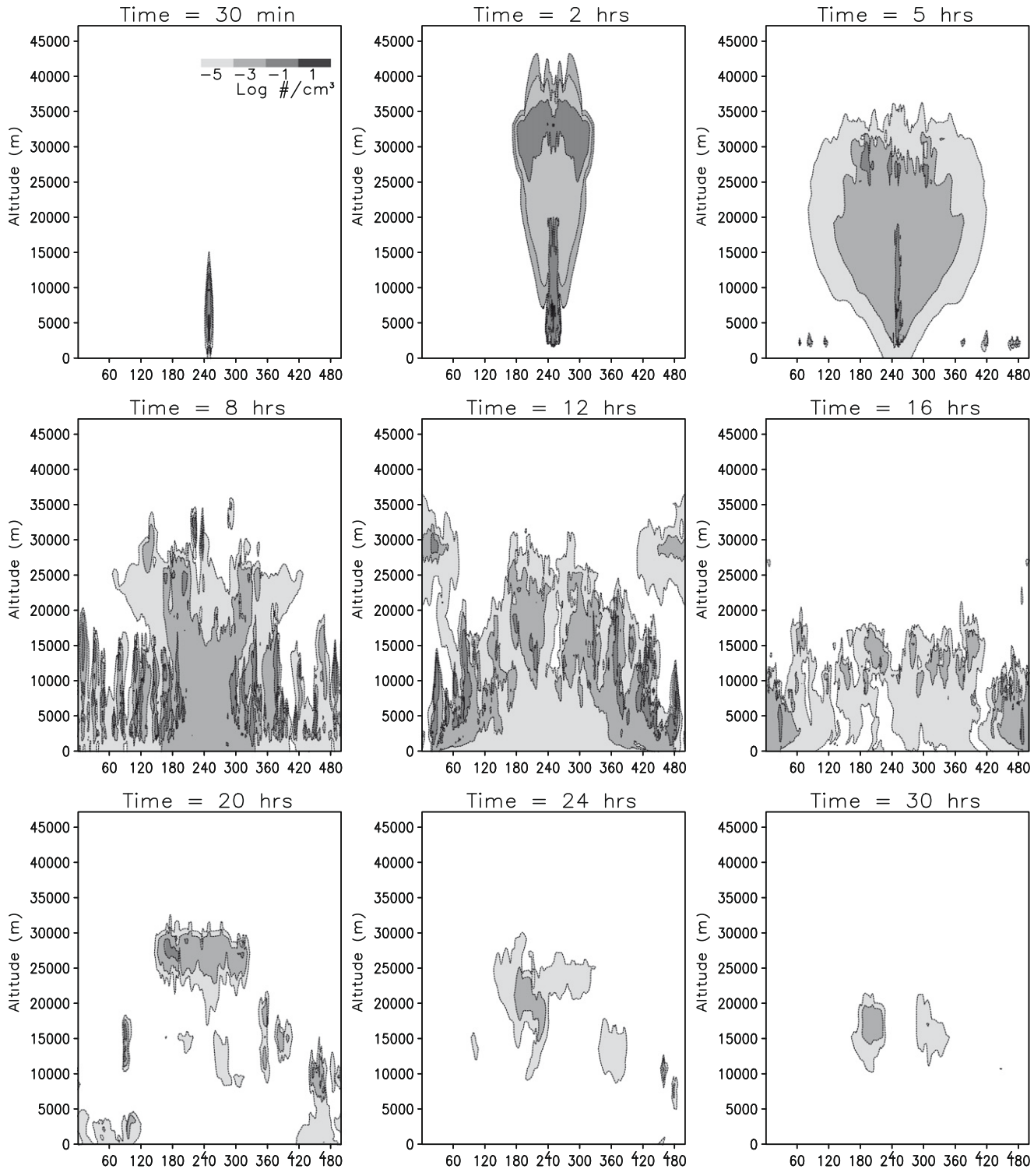

Fig. 4. Time evolution of clouds from a TRAMS simulation for a model initialized with a methane surface humidity of 70%. Contours are the same as in Fig. 2.

slightly supersaturates due to convergence from the cyclical horizontal boundary conditions. These clouds produce a short-lived increase in the overall cloud optical depth (e.g., see Figs. 6–9), but the particles do not survive long enough to affect the accumulation of precipitation at the surface. As time approaches the maximum simulation time of 48 h, fewer clouds form, with the possible loss of all clouds due to rainout and evaporation.

The specific cloud top altitudes, horizontal extent, and cloud lifetimes are strongly tied to the environmental conditions (see Table 2). The surface humidity must be greater than 50% for the cloud top to rise above 30 km and greater than 60% for the cloud top to rise above 35 km. Figs. 6–9 show a series of vertical slices which illustrate the appearance and longevity of cloud features for various altitudes. Optical depths are calculated at 2.16 μm, but given the size of cloud particles, are approximately equivalent to the geometric limit. The portion of the cloud that reaches the highest altitudes is considerably less extensive and shorter lived in time than the clouds at 20 km and lower altitudes. This would explain the

Please cite this article in press as: Barth, E.L., Rafkin, S.C.R. Convective cloud heights as a diagnostic for methane environment on Titan. Icarus (2009), doi:10.1016/j.icarus.2009.01.032

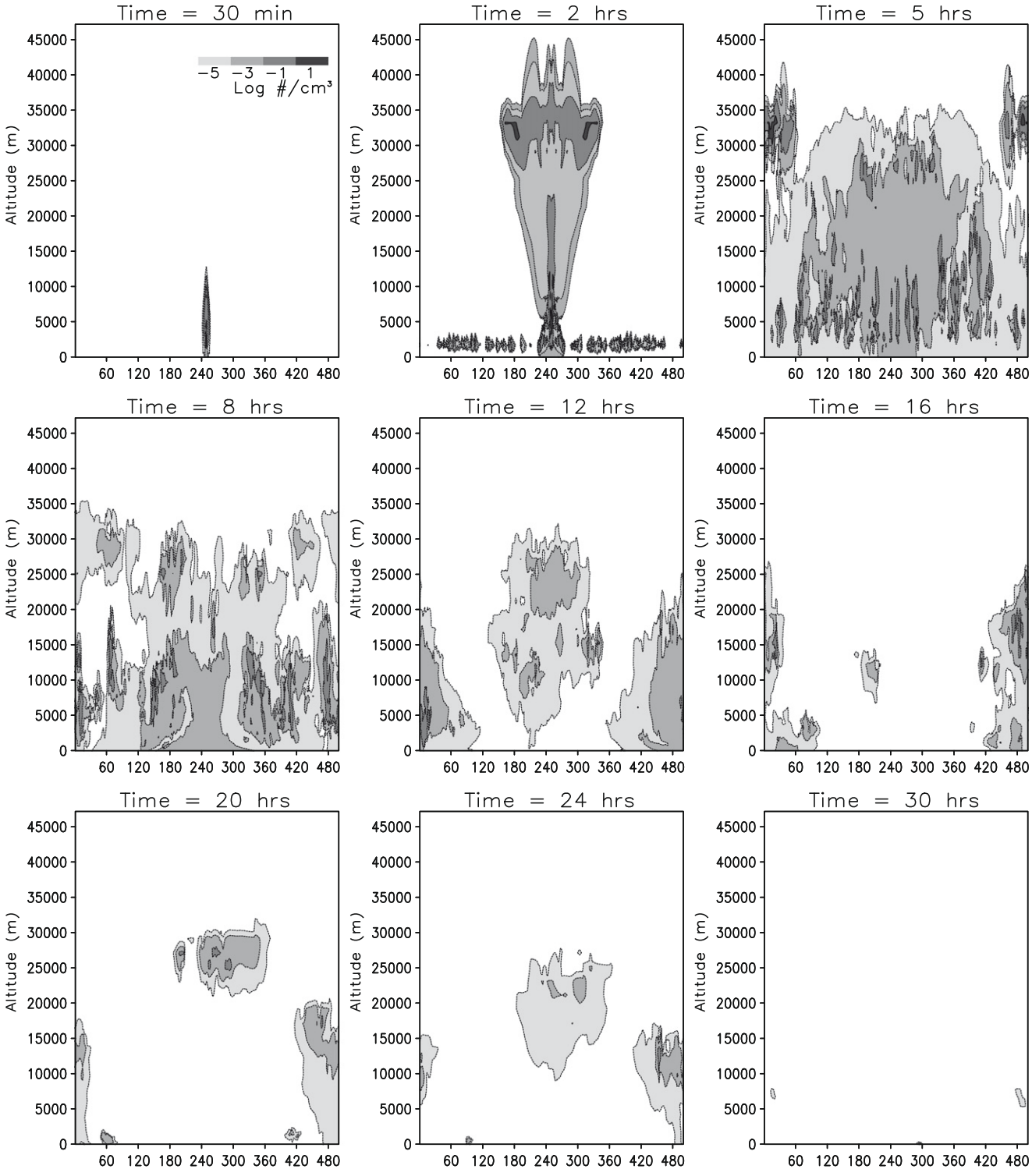

Fig. 5. Time evolution of clouds from a TRAMS simulation for a model initialized with a methane surface humidity of 80%. Contours are the same as in Fig. 2.

lower cloud heights determined by ground-based observations (e.g., Griffith et al., 1998; Brown et al., 2002) as discussed further in Section 4. For the 50% case, clouds are present below 20 km for the entire 2-day simulation, confined to about $x = \pm 100$ km about the center (where the air parcel was initially triggered to rise) and there is some CAPE at the end of the simulation time outside this region. For the higher methane abundance cases, clouds spread horizontally to cover the entire 500 km domain below 20 km altitude in the first day of the simulation, but no CAPE remains at the end of the simulations. The heights of the clouds after their initial rise are consistent with the altitude of the equilibrium level for each methane case. Updraft velocities in the core of the central cloud are between 10 m/s (50% case) and 20 m/s (80% case). Maximum downdraft velocities for all cases are about one third the value of the updraft velocities. Average particle sizes are similar for each case (Figs. 10–13), millimeter-sized particles near the surface and ~100 μm particles at the highest altitudes. The millimeter size particles rarely exist above the 20 km level.

Please cite this article in press as: Barth, E.L., Rafkin, S.C.R. Convective cloud heights as a diagnostic for methane environment on Titan. Icarus (2009), doi:10.1016/j.icarus.2009.01.032

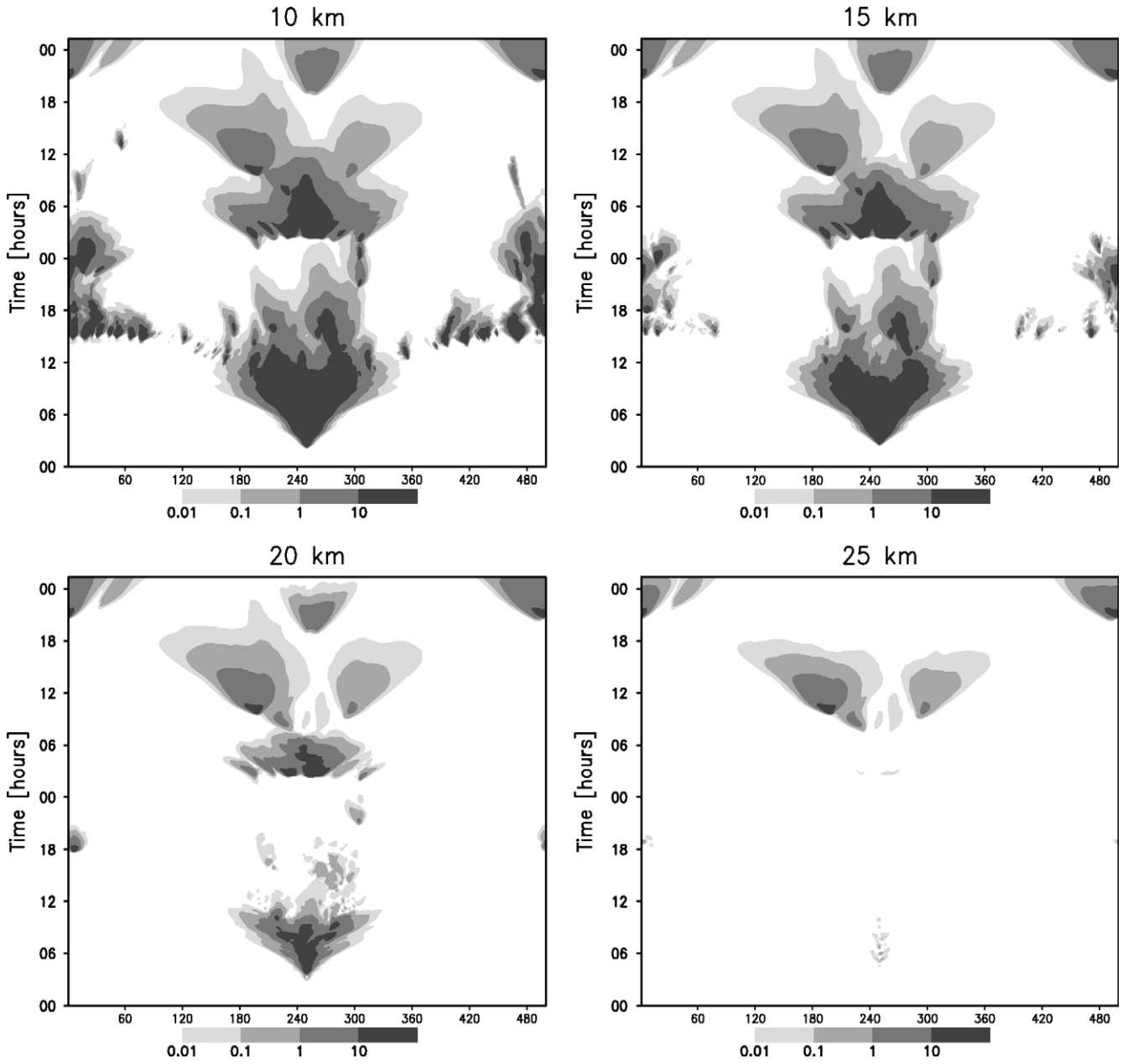

Fig. 6. Vertical slices showing cloud optical depth (shaded contours) as a function of horizontal distance (x-axis, km) and time. The simulation is the same as shown in Fig. 2 (50% humidity case).

3.2. Importance of cloud condensation nuclei and the nucleation barrier

3.2.1. Haze particle size and abundance

Particles from the haze layer serve as condensation nuclei for Titan's clouds. The standard haze profile in TRAMS was generated from a steady-state column microphysics model (Barth and Toon, 2003). This model was run over a vertical domain of 600 km, assuming a haze production function as in Toon et al. (1992). Figs. 14 and 15 show the initial haze particle number density and mean radius as a function of altitude in TRAMS.

Prior to the descent of the Huygens probe in January 2005, it was widely believed that there should be a clearing of haze particles in the troposphere due to condensation of various hydrocarbons. Tomasko et al. (2005) reported observations of haze particles throughout Titan's troposphere from measurements made by the Descent Imager/Spectral Radiometer (DISR) instrument on the Huygens probe. They found that fractal particles with monomer radius of 0.05 μm were necessary to fit the spectra and looked at models with 512 and 256 monomers. The fits for number density of haze particles below 80 km allowed between 20 and 100 cm^{-3}, depending on the wavelength and number of monomers.

After further analysis of the DISR data, Tomasko et al. (2008) found that particles below 30 km could be approximated as spheres with effective radii between 3 and 10 μm, presumably because the haze particles have been coated with hydrocarbons, including methane. For 3 μm particles, the number density is around 0.7 cm^{-3}. Larger particles in the lowest few kilometers require a number density about 10 times smaller to fit the data. In the region of the troposphere above 30 km, number densities are likely to be greater than 5 cm^{-3}.

Please cite this article in press as: Barth, E.L., Rafkin, S.C.R. Convective cloud heights as a diagnostic for methane environment on Titan. Icarus (2009), doi:10.1016/j.icarus.2009.01.032

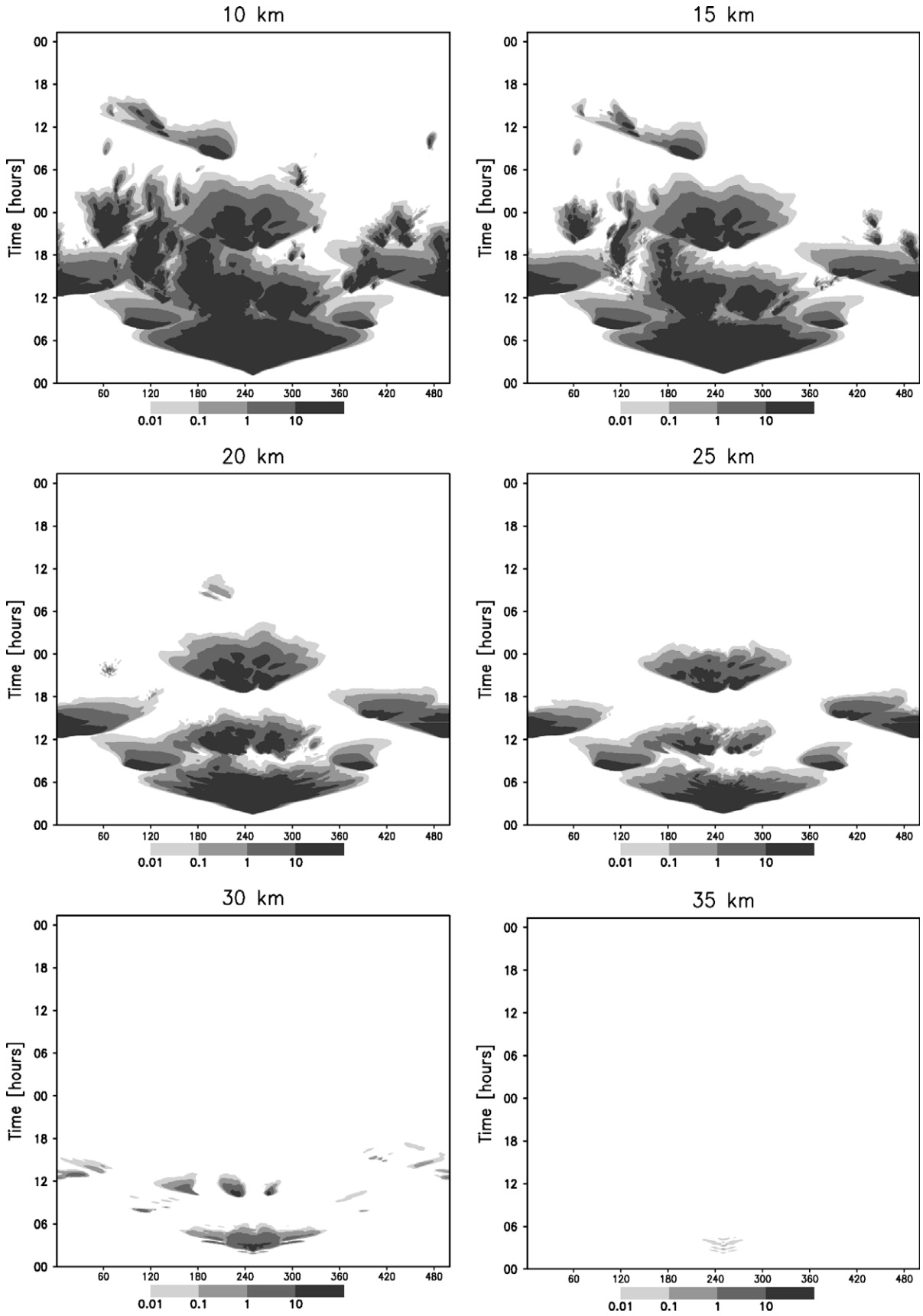

Fig. 7. Vertical slices showing cloud optical depth (shaded contours) as a function of horizontal distance (x-axis, km) and time. The simulation is the same as shown in Fig. 3 (60% humidity case).

Please cite this article in press as: Barth, E.L., Rafkin, S.C.R. Convective cloud heights as a diagnostic for methane environment on Titan. Icarus (2009), doi:10.1016/j.icarus.2009.01.032

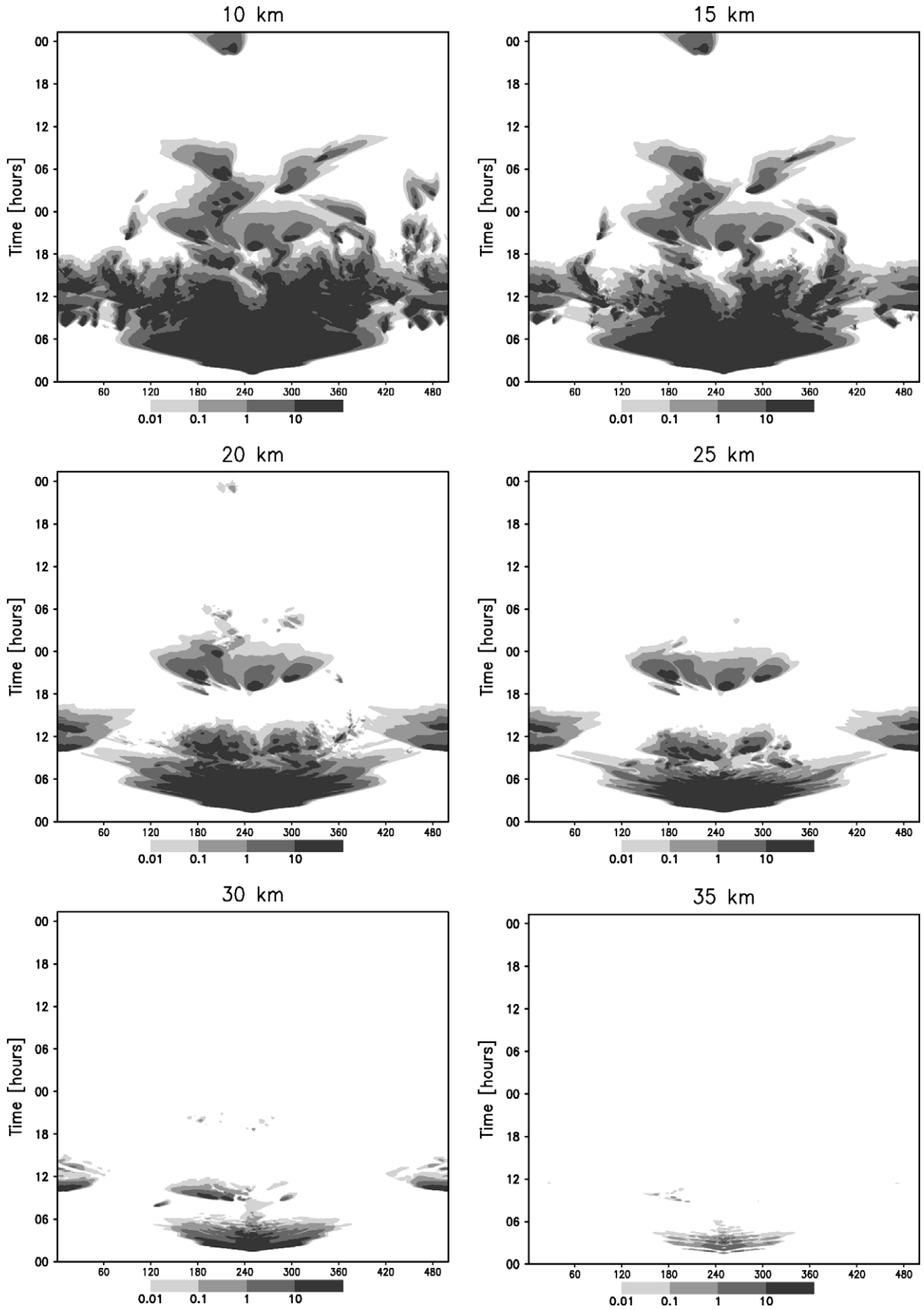

Fig. 8. Vertical slices showing cloud optical depth (shaded contours) as a function of horizontal distance (x-axis, km) and time. The simulation is the same as shown in Fig. 4 (70% humidity case).

Please cite this article in press as: Barth, E.L., Rafkin, S.C.R. Convective cloud heights as a diagnostic for methane environment on Titan. Icarus (2009), doi:10.1016/j.icarus.2009.01.032

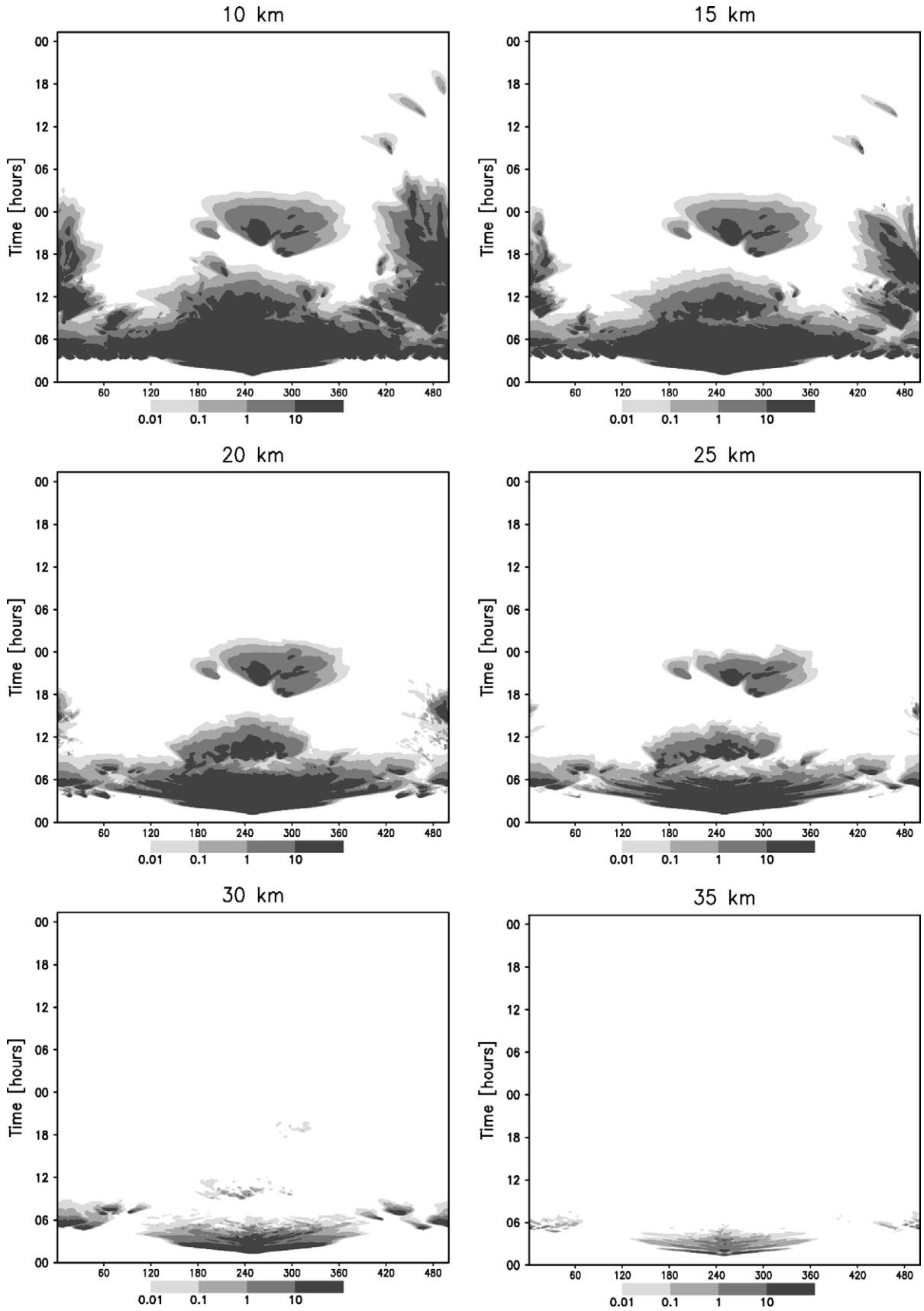

Fig. 9. Vertical slices showing cloud optical depth (shaded contours) as a function of horizontal distance (x-axis, km) and time. The simulation is the same as shown in Fig. 5 (80% humidity case).

Please cite this article in press as: Barth, E.L., Rafkin, S.C.R. Convective cloud heights as a diagnostic for methane environment on Titan. Icarus (2009), doi:10.1016/j.icarus.2009.01.032

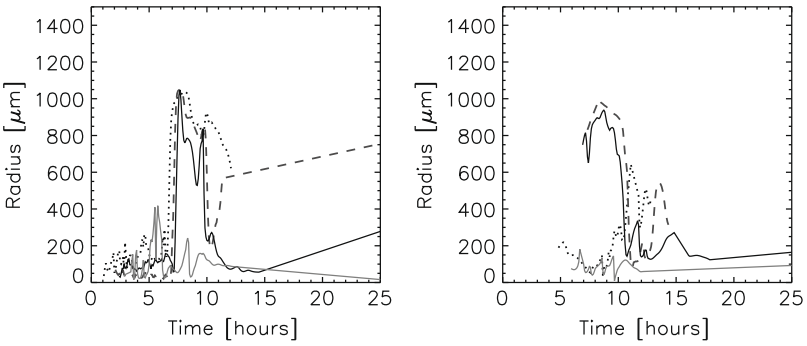

Fig. 10. Average cloud particle radius as a function of time for the 50% surface humidity case. Lines compare various altitudes: 5 km (dotted), 10 km (dashed), 15 km (solid, dark), 20 km (solid, light). The particles shown in the left plot are from the core of the convective cloud (x = 250 km); the right plot shows cloud particles 30 km away from the core (x = 220 km). The average particle size is not calculated when number of particles falls below a threshold of 10^{-8} cm^{-3}.

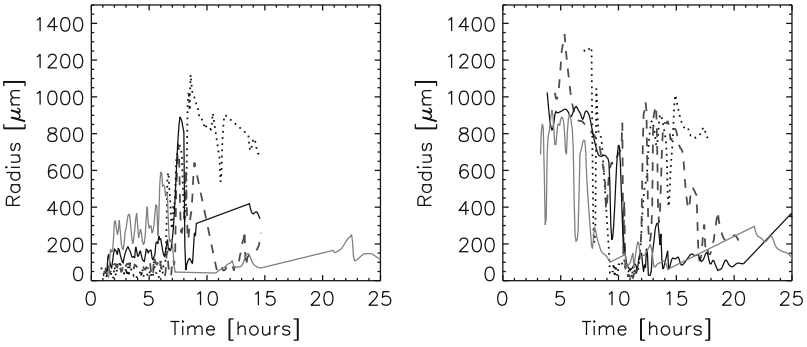

Fig. 11. Average cloud particle radius as a function of time for the 60% surface humidity case. Lines compare various altitudes: 5 km (dotted), 10 km (dashed), 15 km (solid, dark), 20 km (solid, light). The particles shown in the left plot are from the core of the convective cloud (x = 250 km); the right plot shows cloud particles 50 km away from the core (x = 200 km). The average particle size is not calculated when number of particles falls below a threshold of 10^{-8} cm^{-3}.

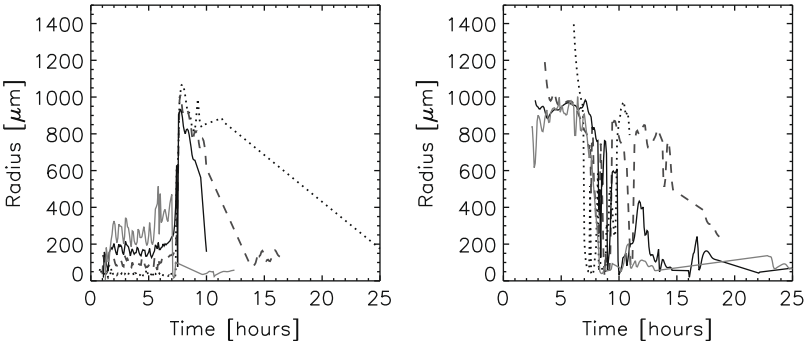

Fig. 12. Average cloud particle radius as a function of time for the 70% surface humidity case. Lines compare various altitudes: 5 km (dotted), 10 km (dashed), 15 km (solid, dark), 20 km (solid, light). The particles shown in the left plot are from the core of the convective cloud (x = 250 km); the right plot shows cloud particles 50 km away from the core (x = 200 km). The average particle size is not calculated when number of particles falls below a threshold of 10^{-8} cm^{-3}.

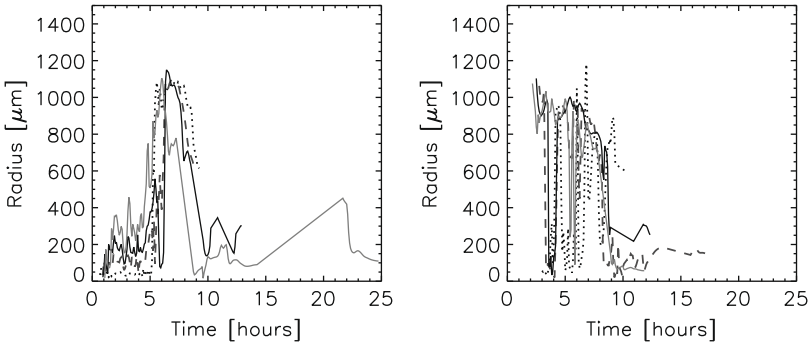

Fig. 13. Average cloud particle radius as a function of time for the 80% surface humidity case. Lines compare various altitudes: 5 km (dotted), 10 km (dashed), 15 km (solid, dark), 20 km (solid, light). The particles shown in the left plot are from the core of the convective cloud (x = 250 km); the right plot shows cloud particles 50 km away from the core (x = 200 km). The average particle size is not calculated when number of particles falls below a threshold of 10^{-8} cm^{-3}.

Please cite this article in press as: Barth, E.L., Rafkin, S.C.R. Convective cloud heights as a diagnostic for methane environment on Titan. Icarus (2009), doi:10.1016/j.icarus.2009.01.032

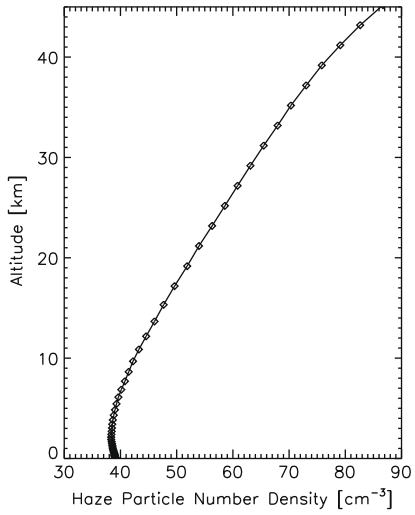

Fig. 14. Number density profile for haze particles to initialize a column of atmosphere in TRAMS using the steady-state output from the Titan-CARMA column microphysics model.

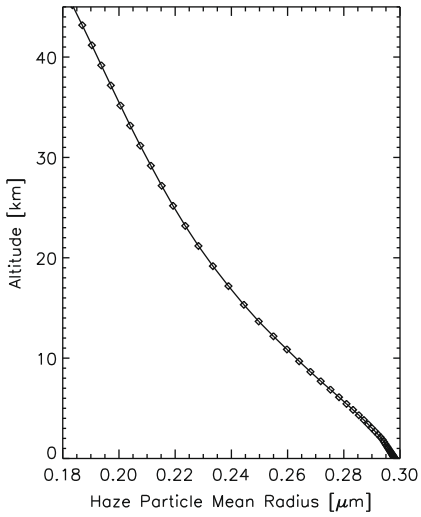

Fig. 15. Mean radius profile for haze particles to initialize a column of atmosphere in TRAMS using the steady-state output from the Titan-CARMA column microphysics model.

We look at the effects of haze particle size and number density by running a number of simulations with one haze size bin representing the effective radius of the particles (tests include 0.4, 0.8, 1.2 and 2.4 μm; these particular sizes were chosen to maintain a mass ratio of 8 between bins and not exceed ~4.5 mm radius for the largest cloud bin) and constant number density with altitude (N values are 1, 2, 10, 20, and 50 cm^{-3}). The flux of haze particles into the top boundary of the model is the fall velocity multiplied by the number of particles. 50 cm^{-3} is slightly more than 85% of the haze particle column abundance in our standard model (Fig. 14); 1 cm^{-3} has a column abundance of less than 2% that of our standard model.

The size of the haze particles does not affect the appearance of the clouds. The number of haze particles only begins to limit the maximum vertical extent of the clouds for $N \leqslant 10$ cm^{-3}, but only by 1 vertical level (2 km). For N = 1–2 cm^{-3}, the clouds have a smaller horizontal extent by 30 to 60 km. This is not surprising as the number of cloud particles necessary for an optical depth of one is less than 1 cm^{-3}. Also, haze particles are small enough that they essentially transport only through atmospheric motions and so as air is pulled into the core of the cloud, haze particles are as well. The effects of varying the haze abundance and particle size are summarized in Table 3.

Table 3
Changes in cloud properties for various sensitivity tests.

Model	Max cloud top	Time/Cloud Activity	Horizontal extent
Haze particles			
Change r_{eff}	No change	No change	No change
N = 20–50 cm^{-3}	No change	No change	+40 km at max cloud top, same below
N = 5–10 cm^{-3}	−2 km	No change	No change
N = 1,2 cm^{-3}	−2 to 4 km	No change	−40 km
Scrit			
less than 1.10	No change	More clouds	Later clouds greater horiz extent
greater than 1.10	−8 km	Less to no clouds in day 2	−30 to 60 km
Coalescence			
No coales	+4 km	Longer lifetime	Fills entire 500 km domain at $z \lesssim$ 26–28 km for $t \gtrsim$ 24 hrs
E_{coal} = 10%	+4 km	Longer time at	+60 to 80 km below 30 km
E_{coal} = 25%	+2 km	Higher altitudes	Similar to 10% case
E_{coal} = 50%	No change	+ few hours	+20 km
E_{coal} = 100%	No change	No change	No change
E_{coal} = BO84[a]	+2 km	Similar to 50% case	Similar to 50% case
E_{coll} = L48[a]	-2 km	Few hours longer below 30 km	−40 km
$E^{*}_{coal}E_{coll} = 100\%$	−6 km	No change	Confined to ~ ± 50 km from center

[a] Beard and Ochs (1984), Langmuir (1948).

3.2.2. Critical saturation for methane nucleation

Barth and Toon (2003) describes the equations governing the nucleation process. The critical saturation, S_{crit}, quantifies the ease with which nucleation will occur, such that S_{crit} = 1.0 means the nucleation rate is 1 cm^{-2} s^{-1} at saturation. Lab measurements of the critical saturation for nucleation of methane (ice) onto tholin indicate a critical saturation of less than or equal to 1.10 for a measurement temperature of 45 K (D. Curtis, private communication; recently updated to 1.07 ± 0.008, Curtis et al., 2008). For simplicity, we use the same critical saturation for nucleation of methane as both ice and liquid.

When the nucleation barrier is completely lifted, a single cloud forms and rises in the center of the model domain, but completely evaporates within about half a day. The competing effects of nucleation and evaporation keep the cloud particles from growing bigger than about 100 μm. Particles of this size are too small to fall back to lower altitudes and trigger additional cloud formation, so only the methane in the near environment to the cloud ever contributes to the cloud forming process. The methane environment more than about 10 km away from the cloud is unaffected, so the rest of the methane reservoir is never tapped and the cloud is short-lived. The cloud never extends enough in the horizontal direction to reach the resolution of the VIMS instrument aboard Cassini.

However, for any barrier to nucleation, cloud particles are able to grow sufficiently large before the atmosphere becomes subsaturated and can support additional cloud formation at a later time. For S_{crit} values less than our nominal value (1.01–1.05), the highest cloud top altitude remains the same as the 1.10 (nominal) case, but

Please cite this article in press as: Barth, E.L., Rafkin, S.C.R. Convective cloud heights as a diagnostic for methane environment on Titan. Icarus (2009), doi:10.1016/j.icarus.2009.01.032

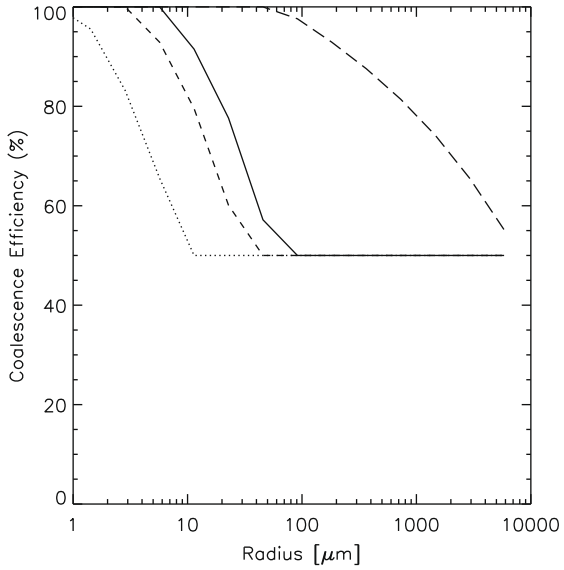

Fig. 16. Coalescence efficiencies for the cloud particles in the model using data from Beard and Ochs (1984). Curves are for sizes of one of the colliding particles with diameters of: 5 mm (dots), 500 μm (short dashes), 100 μm (solid), and 10 μm (long dashes). The total efficiency for gravitational collection is the product of the collision efficiency and the coalescence efficiency.

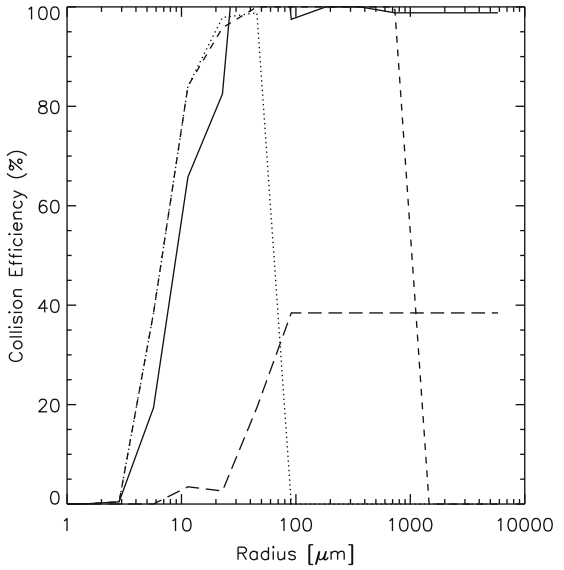

Fig. 17. Collision efficiencies for the cloud particles in the model using data from Beard and Ochs (1984). Curves are for sizes of one of the colliding particles with diameters of: 5 mm (dots), 500 μm (short dashes), 100 μm (solid), and 10 μm (long dashes). The total efficiency for gravitational collection is the product of the collision efficiency and the coalescence efficiency.

horizontal extent of clouds is increased. Once a cloud is formed, the nucleation process must compete with the condensation process for the available methane supply. Since condensation occurs once the environment reaches saturation (though effects of droplet curvature can force evaporation of the smallest sizes even in a saturated atmosphere), it becomes much harder for nucleation to form more cloud particles as S_{crit} increases. As a consequence, for cases with higher S_{crit} values (1.15–1.30), cloud particles are fewer in number and grow larger and so do not rise as high in the atmosphere. The horizontal extent and lifetime of the clouds also decreases as S_{crit} increases. Table 3 summarizes the results described above.

3.3. Coalescence of cloud particles

The high vapor pressure of methane makes condensation an efficient process for growing cloud particles up to radii of several 100 μm. Further growth of cloud particles, up to several millimeters in diameter, requires a sufficient number of particles for collisions to take place. Gravitational collection describes this process. The coagulation kernel for gravitational collection is

$$K_{coag} = E_{coal} E_{coll} \pi (r_l + r_s)^2 (v_{fl} - v_{fs}), \tag{10}$$

where r_l and r_s are the radii of the two colliding particles which fall with velocities v_{fl} and v_{fs}. The collection efficiency is the product of the coalescence efficiency, E_{coal} - the fraction of collisions which result in coalescence, and the collision efficiency, E_{coll} - the probability of a collision between two drops. Most laboratory studies of coalescence efficiency have been motivated by terrestrial meteorology and so are specific to water droplets (e.g., Beard and Ochs, 1984). Given the differences in viscosity and surface tension between water and hydrocarbon droplets, it is not clear how well water droplet data will apply to coalescence of cloud particles in Titan's atmosphere. Post and Abraham (2002) calculate a coalescence efficiency for hydrocarbon droplets using the Weber number,

$$E_{coal} = \min\left(1.0, \frac{2.4 f(y)}{We}\right), \tag{11}$$

where $f(y) = y^3 - 2.4\,y^2 + 2.7y$ is a function of the ratio of the colliding particle radii ($y = r_l/r_s$). The Weber number compares the inertial force to the surface force,

$$We = \frac{\rho_{drop}(v_{fl} - v_{fs})^2 2 r_s}{\sigma_{lv}}, \tag{12}$$

where ρ_{drop} is the density of the droplet and σ_{lv} is the droplet surface tension.

For similar size droplets falling at the same velocity, the ratio of We_{CH_4} to We_{H_2O} is about 1.5. However, on Titan droplets fall more slowly by about a factor of 5 (Lorenz, 1993), so We_{CH_4} will be much smaller than We_{H_2O}. For Titan conditions and expected particle sizes, the Weber number coalescence efficiency tends toward 100%.

The collision efficiency is the ratio of the collision cross section πy_c^2 to the geometric cross-section $\pi\ (r_s + r_l)^2$. The collision efficiency is generally approximated from laboratory experiments. Beard and Ochs (1984) tabulated collision efficiencies based on the numerical calculations of Beard and Grover (1974), which apply to atmospheric pressures found throughout much of Titan's troposphere. Figs. 16 and 17 shows the Beard and Ochs (1984) coalescence and collision efficiencies for various particle sizes.

Barth and Toon (2006) found coalescence to be negligible in their optically thin methane and ethane clouds (particle numbers were of order 10^{-4} cm^{-3}, severely limiting the number of collisions). However, the greater number densities in convective clouds (e.g., Barth and Rafkin, 2007) increase the likelihood of collisions and coalescence is necessary to grow droplets large enough to create abundant precipitation. A number of simulations spanning possible coalescence and collision efficiencies are summarized in Table 3. Coalescence efficiencies were (1) set to radius independent values between 0 and 100%, (2) calculated from the data of Beard and Ochs (1984), or (3) calculated from the Weber number following Eq. (11). Collision efficiencies were determined based on either the calculations of Beard and Ochs (1984) or Langmuir (1948) (significantly higher collision rates for most sizes, especially >100 μm).

Average particle sizes are much smaller when there is no coagulation - only briefly do we see 500–1000 μm particles and only at altitudes of 5 km or less. For the (E_{coal}=) 10% and 25% cases below 5 km particles can reach radii ~800 μm for

Please cite this article in press as: Barth, E.L., Rafkin, S.C.R. Convective cloud heights as a diagnostic for methane environment on Titan. Icarus (2009), doi:10.1016/j.icarus.2009.01.032

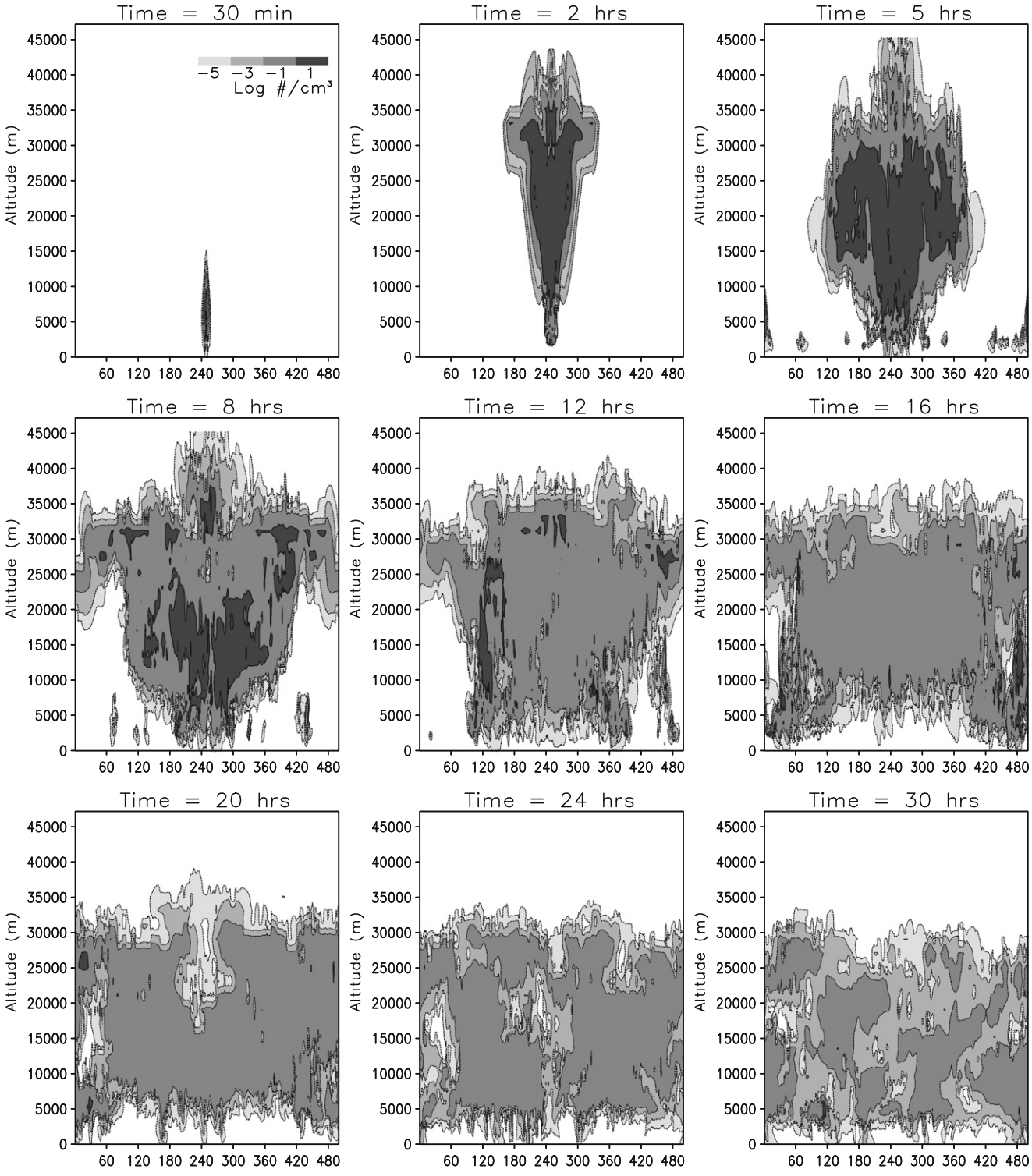

Fig. 18. Time evolution of clouds from a model initialized with a methane surface humidity of 70% but with no coalescence of cloud particles. Contours show the number density of cloud particles (number density in cm^{-3}). Contour labels are log of number density (−5, −3, −1, 0, 1); shading darkens with increased number. The contour labels were removed from the second row of plots for clarity, but shading is consistent for all plots. Clouds are below optical depth of 0.1 for $N \lesssim 10^{-3}$ cm^{-3}.The simulation is similar to that shown in Fig. 4 (70% humidity case) but assuming no coalescence of cloud particles.

about half a day but are mostly $\lesssim$200 μm at 20 km, and rarely to never reach sizes of 500 μm. In each of these cases, the smaller particle sizes allow for higher peak altitudes, by 2 to 4 km. Figs. 18 and 19 illustrate the higher cloud tops and significant increase in cloud particle abundance for a no coalescence case with a 70% methane environment. Below 20 km, clouds are visible for the entire 2 day simulation. For $E_{coal} > 50\%$, the clouds remain relatively unchanged. When the collision efficiency is increased following the formula of Langmuir (1948), cloud tops are lowered by 2 km. Assuming the entire collection process is 100% efficient, peak altitudes are reduced by 6 km. These results are summarized in Table 3.

Please cite this article in press as: Barth, E.L., Rafkin, S.C.R. Convective cloud heights as a diagnostic for methane environment on Titan. Icarus (2009), doi:10.1016/j.icarus.2009.01.032

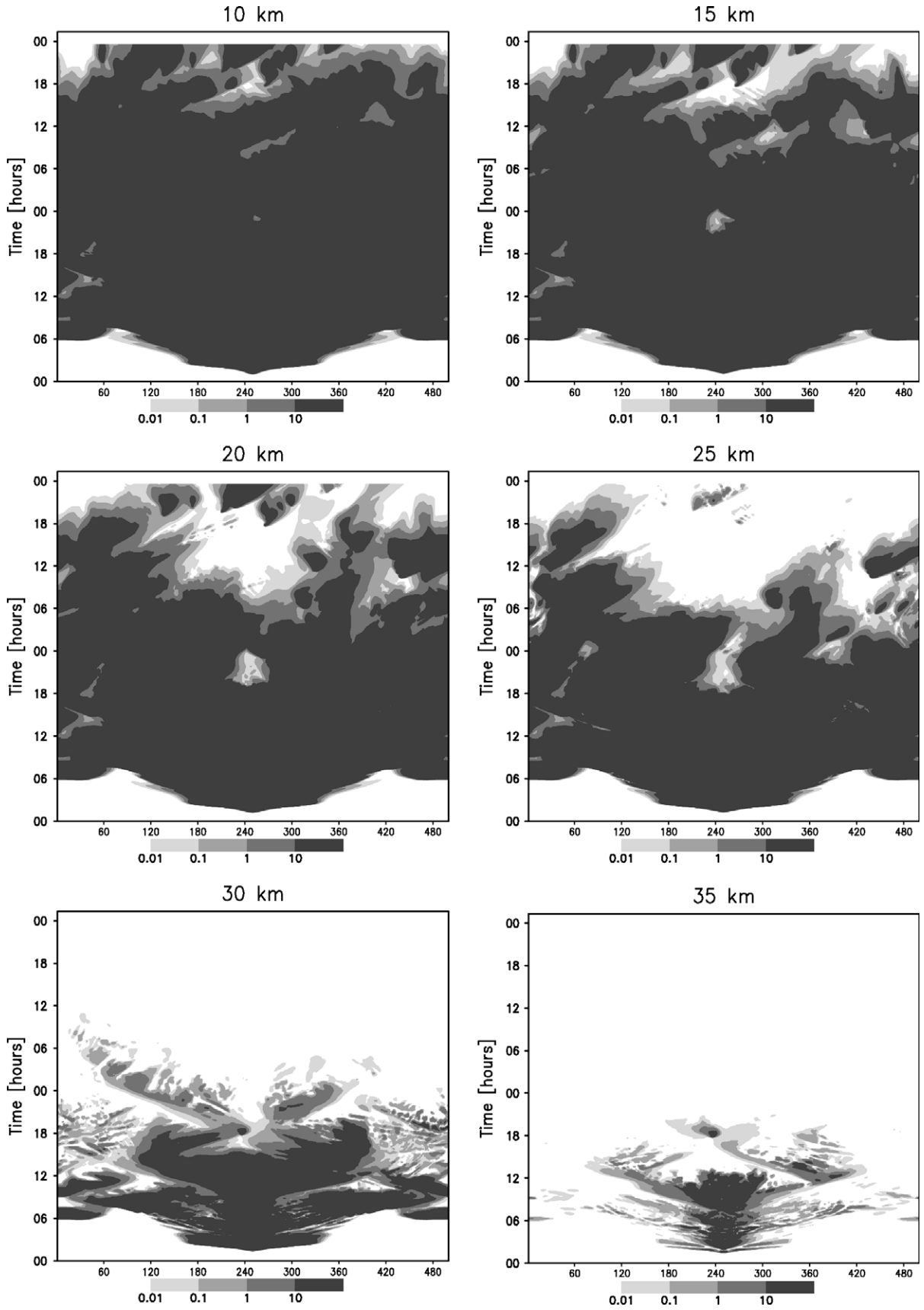

Fig. 19. Vertical slices showing cloud optical depth (shaded contours) as a function of horizontal distance (*x*-axis, km) and time for the simulation shown in Fig. 18. The simulation is similar to that shown in Fig. 8 (70% humidity case) but assuming no coalescence of cloud particles.

Please cite this article in press as: Barth, E.L., Rafkin, S.C.R. Convective cloud heights as a diagnostic for methane environment on Titan. Icarus (2009), doi:10.1016/j.icarus.2009.01.032

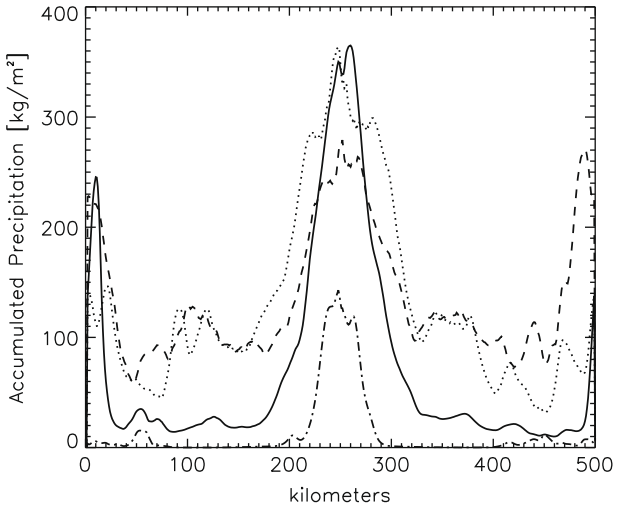

Fig. 20. Accumulated precipitation for the four methane abundance cases. The coalescence efficiency is calculated using the Weber number. Lines indicate different initial methane abundance values defined by surface humidity of 50% (dash-dot), 60% (solid), 70% (dot), and 80% (dash). Dividing the accumulation amounts by a factor of 4 gives the approximate column of methane produced in centimeters.

4. Implications for cloud observations and precipitation

Griffith et al. (2005) report the highest cloud tops at 42 km. Uncertainties in their methane abundances by up to a factor of 2 could change the cloud altitudes by 5 km and the derived optical depths by 20%. It is clear that for any reasonable amount of methane in the environment, such high cloud tops are the result of overshooting the equilibrium level. From the simulations described above, these convective overshoots can reach ~10 km above the anvil portion of the cloud. Nevertheless, we find that the appearance of clouds so close to the tropopause indicates a much more humid surface environment (*e.g.* surface mole fraction increased by factors of ~1.5–1.75) at mid-latitudes than was found at the Huygens landing site.

Ground-based observations find cloud tops at much lower altitudes (around 20 km or lower). Our simulations show this to be the case given the poorer resolution ($\gtrsim 100$ km) of ground-based telescopes compared to Cassini. However, the lifetimes of the clouds simulated here rarely exceed one day, which is shorter than seen by the observations described in Section 1. In most of the simulations, particularly those with the highest methane abundances, there is little to no Convective Available Potential Energy (CAPE) left after the first day and so further cloud formation will not occur. The lifetime of the clouds is then controlled by the sedimentation times of the particles. Only the smaller particles in the no coalescence cases can remain aloft to be visible for the entire two days. In the real world, CAPE is presumably re-supplied by large-scale forcing and longer lived cloud systems may be sustained.

One factor that could serve to decrease the effectiveness of coalescence for methane cloud particles in Titan's atmosphere is the fraction of particles in the cloud which are still mostly frozen. If ice particles are falling through a subsaturated atmosphere, evaporative cooling is generally sufficient to keep the temperature of the particle above the melting point. Another issue is the melting point temperature of a methane cloud particle. Pure methane ice melts at a temperature of 90.6 K, but if the the particle initially forms as a liquid droplet and then freezes, some N_2 may still be present and melting may occur at lower temperatures. Nevertheless, it is likely that a large fraction of the cloud particles in the lower half of Titan's troposphere are still frozen.

One puzzle that has been brought to light through Cassini observations is why are lakes present in the northern hemisphere, but active cloud formation is only seen in the southern hemisphere? The simulations presented here all produce some amount of precipitation. Those shown in Figs. 2–5, produce ~1/2 to a few meters of methane accumulation. Only the convective clouds produce any precipitation. Fig. 20 compares the accumulation for the different methane environments. The curves are shown for the entire two day simulation, though precipitation ceases after the first 12 h (except near horizontal boundaries). The additional methane in the atmosphere and humidity at the surface allows for a larger accumulation of precipitation at the surface. Surface evaporation is inefficient to compete with the rainfall. Simulations with and without the surface evaporation process turned on do not differ significantly. Precipitation decreases by greater than a factor of 10 when the coalescence process is completely turned off. This is true for all the methane environments. As an example, at the end of the two day simulation for the 70% case, the accumulation of methane rain in any grid cell is only a few centimeters.

5. Conclusions

We have conducted a number of simulations with our Titan Regional Atmospheric Modeling System (TRAMS) to explore the sensitivity of various microphysics and environmental parameters to the appearance of Titan's convective clouds. We find that the amount of methane in the atmosphere is the most significant factor in influencing the height of the cloud tops and that the appearance of mid-latitude clouds near the tropopause implies a much wetter environment than was measured at the Huygens landing site. The other important factor affecting cloud top heights is the efficiency with which cloud particles coalesce, which may be low given large fractions of ice particles in the clouds. Both of these factors have significant implications for the amount of precipitation produced by Titan's convective clouds.

Acknowledgment

This project was supported through the NASA Planetary Atmospheres Program Grant NNX07AJ14G.

Appendix A. Supplementary data

Convective cloud heights as a diagnostic for methane environment on Titan

The movies follow the time evolution of four TRAMS cloud simulations corresponding to the panels shown in Figs. 2–5 in the text. Altitude in meters is on the *y*-axis and horizontal distance in kilometers is on the *x*-axis. Colored contours indicate the number density of clouds particles (values on color bar are log(*N*), where *N* has units of cm^{-3}). Time is given in hours (note that the time increment between frames increases after the first 12 h shown). In each case the clouds follow a similar pattern of formation and dissipation but differ in horizontal extent, cloud top height, and longevity related to the initial amount of methane in the atmosphere. A full description of the cloud lifecycle can be found in Section 3.1 of the text. Supplementary data associated with this article can be found, in the online version, at doi:10.1016/j.icarus.2009.01.032.

References

Barth, E.L., Rafkin, S.C., 2007. TRAMS: A new dynamic cloud model for Titan's methane clouds. Geophys. Res. Lett. 34, L03203.

Barth, E.L., Toon, O.B., 2003. Microphysical modeling of ethane ice clouds in Titan's atmosphere. Icarus 162, 94–113.

Please cite this article in press as: Barth, E.L., Rafkin, S.C.R. Convective cloud heights as a diagnostic for methane environment on Titan. Icarus (2009), doi:10.1016/j.icarus.2009.01.032

Barth, E.L., Toon, O.B., 2006. Methane, ethane, and mixed clouds in Titan's atmosphere: Properties derived from microphysical modeling. Icarus 182, 230–250.

Beard, K.V., Grover, S.N., 1974. Numerical collision efficiencies for small raindrops colliding with micron size particles. J. Atmos. Sci 31, 543–550.

Beard, K.V., Ochs, H.T., 1984. Collection and coalescence efficiencies for accretion. J. Geophys. Res. 89, 7165–7169.

Bouchez, A.H., Brown, M.E., 2005. Statistics of Titan's south polar tropospheric clouds. Astrophys. J. 618, L53–L56.

Brown, M.E., Bouchez, A.H., Griffith, C.A., 2002. Direct detection of variable tropospheric clouds near Titan's south pole. Nature 240, 795–797.

Curtis, D.B., Hatch, C.D., Hasenkopf, C.A., Toon, O.B., Tolbert, M.A., McKay, C.P., Khare, B.N., 2008. Laboratory studies of methane and ethane adsorption onto organic particles: Application to Titan's clouds. Icarus 195, 792–801.

Fulchignoni, M., and 42 colleagues, 2005. In situ measurements of the physical characteristics of Titan's environment. Nature 438, 785–791.

Graves, S., McKay, C., Griffith, C., Ferri, F., Fulchignoni, M., 2008. Rain and hail can reach the surface of Titan. Planet. Space Sci. 56, 346–357.

Griffith, C.A., Owen, T., Miller, G.A., Geballe, T., 1998. Transient clouds in Titan's lower atmosphere. Nature 395, 575–578.

Griffith, C.A., Penteado, P., Baines, K., Drossart, P., Barnes, J., Bellucci, G., Brown, R., Buratti, B., Capaccioni, F., Cerroni, P., Clark, R., Combes, M., Coradini, A., Cruikshank, D., Formisano, v., Jaumann, R., Langevin, Y., Matson, D., McCord, T., Mennella, V., Nelson, R., Nicholson, P., Sicardy, B., Sotin, C., Soderblom, L.A., Kursinski, R., 2005. The Evolution of Titan's Mid-Latitude Clouds. Sc ience 310, 474–477.

Hueso, R., Sánchez-Lavega, A., 2006. Methane storms on Saturn's moon Titan. Nature 442, 428–431.

Langmuir, I., 1948. The production of rain by a chain reaction in cumulus clouds at temperatures above freezing. J. Meteor 5, 175–192.

Lorenz, R.D., 1993. The life, death and afterlife of a raindrop on Titan. Planet. Space Sci. 41, 647–655.

Nicholls, M.E., Pielke, R.A., 2000. Thermally induced compression waves and gravity waves generated by convective storms. J. Atmos. Sci. 57, 3251–3271.

Porco, C.C., and 35 Colleagues, 2005. Imaging of Titan from the Cassini spacecraft. Nature, 434, 159–168.

Post, S.L., Abraham, J., 2002. Modeling the outcome of drop-drop collisions in Diesel sprays. International Journal of Multiphase Flow 28, 997–1019.

Rafkin, S., Haberle, R., Michaels, T., 2001. The Mars Regional Atmospheric Modeling System: Model description and selected simulations. Icarus 151, 228–256.

Roe, H., Pater, I.D., Macintosh, B., McKay, C., 2002. Titan's clouds from Gemini and Keck adaptive optics imaging. Astrophys. J. 581, 1399–1406.

Roe, H.G., Bouchez, A.H., Trujillo, C.A., Schaller, E.L., Brown, M.E., 2005a. Discovery of temperate latitude clouds on Titan. Astrophys. J. 618, L49–L52.

Roe, H.G., Brown, M.E., Schaller, E.L., Bouchez, A.H., Trujillo, C.A., 2005b. Geographic control of Titan's mid-latitude clouds. Science 310, 477–479.

Schaller, E., Brown, M., Roe, H., Bouchez, A., Trujillo, C., 2006a. Dissipation of Titan's South Polar Clouds. Icarus 184, 517–523.

Schaller, E., Brown, M., Roe, H., Bouchez, A., 2006b. A large cloud outburst at Titan's south pole. Icarus 182, 224–229.

Thompson, W.R., Zollweg, J.A., Gabis, D.H., 1992. Vapor-liquid equilibrium thermodynamics of N_2 + CH_4: Model and Titan applications. Icarus 97, 187–199.

Tomasko, M., and 39 colleagues, 2005. Rain, winds and haze during the Huygens probe's descent to. Titan's surface. Nature 438, 765–778.

Tomasko, M., Doose, L., Engel, S., Dafoe, L.E., West, R., Lemmon, M., Karkoschka, E., See, C., 2008. A model of Titan's aerosols based on measurements made inside the atmosphere. Planet. Space Sci. 56, 669–707.

Toon, O.B., McKay, C.P., Griffith, C.A., Turco, R.P., 1992. A physical model of Titan's aerosols. Icarus 95, 24–53.

Please cite this article in press as: Barth, E.L., Rafkin, S.C.R. Convective cloud heights as a diagnostic for methane environment on Titan. Icarus (2009), doi:10.1016/j.icarus.2009.01.032